Particle Accelerators, 1991, Vol. 35, pp. 83–99
Reprints available directly from the publisher
Photocopying permitted by license only

THE ANALYTICAL SOLUTION OF WAKE-FIELDS IN AN ELLIPTICAL PILLBOX CAVITY

J. S. YANG and K. W. CHEN

Center for Accelerator Science and Technology, The University of Texas at Arlington, Arlington, TX 76019

(Received October 26, 1989; in final form June 26, 1990)

The wake potential of a bunch of relativistic charged particles traversing an elliptical pillbox cavity is derived analytically in the limit of vanishing aperture. It is found that the resonant modes of an elliptical cavity can be expressed in terms of Mathieu functions. Calculation results are presented and compared with numerical ones.

1. INTRODUCTION

The wake-field produced by a bunch of relativistic charged particles in an elliptical pillbox cavity is important not only for future high gradient electron accelerators[1], but also for a use as an electric wiggler for some proposed free electron laser schemes[2]. The suitability is based on the estimation that the acceleration gradient will exceed 100 MeV/m per μC of driving bunch charge, and on wavelengths of the order of a few centimeters.

The principle of acceleration by the wake-field generated in a metallic cavity has been experimentally verified[3]. Also, other wake-field acceleration schemes using a plasma medium[4] or a dielectric-loaded cavity[5] have been experimentally investigated. However, these wake-field schemes have not been demonstrated to have significantly larger acceleration gradient than that in a metallic cavity. Elliptical cavities have been investigated by several authors[1,2,6,9]. It was shown[6,9] that in elliptical cavities the transformer ratios are rather limited, and that a strong transverse wake-field, which might lead to beam instabilities, is also excited. However, we can overcome the low transformer ratio and the transverse deflection problem by using multi-stage schemes. Although the transformer ratio would not be as high, a wake-field accelerator not based on the impedance transformation principle could be achieved by using multi-stage schemes with short stages; the driving beam is replaced with a new one or replenished in energy after each stage. By rotating subsequent groups of cavities, the overall transverse deflection of the accelerated beam can be minimized.

The wake potential in an elliptical cavity can be obtained either by modal analysis or by numerically solving Maxwell's equations in the time domain. In the previous modal analysis[7,8], the wake-field is expressed in a Fourier series based on the vector eigenfunctions of the unit pillbox. For infinitely repeating structures, the problem for

the entire acceleration cavity is reduced to that in a pillbox cavity by using Floquet's theorem on the periodicity. The modal analysis can be generalized to a cavity of arbitrary shape when we can calculate the resonant modes. For a cavity with finite apertures we should use numerical methods to find resonant modes accurately. Previously the wake-fields in an elliptic pillbox cavity with finite aperture were calculated using the numerical code WELL[9], which directly solves Maxwell's equations in the time domain.

In this article, we do not take into account the aperture effect. The analytic solution which will be formulated in this article exists and is of interest, even though it is an approximation for the cavity with beam holes, since we can readily estimate the maximum energy gain of the accelerated particle. In view of these considerations, we try to obtain an analytic expression for the resonant modes in an elliptical pillbox cavity in the limit of vanishing aperture. Using the mode analysis, the longitudinal and transverse wake potentials are derived in terms of Mathieu functions. It is also shown that we can derive exactly the same expressions for the wake potentials in a circular cavity as in Ref. 7 when the ellipse tends to a circle.

2. ELLIPTIC PILLBOX CAVITY

2.1. Solution of Homogeneous Helmholtz Equation in an Elliptic Cavity

Consider an elliptic pillbox cavity as shown in Fig. 1. For a cavity of elliptic cross section, the eigenfunctions can be found in terms of known functions by transforming the Cartesian coordinates to the confocal elliptic coordinates as shown in Fig. 2. In these coordinates, boundary conditions on the elliptic cavity are readily satisfied. The

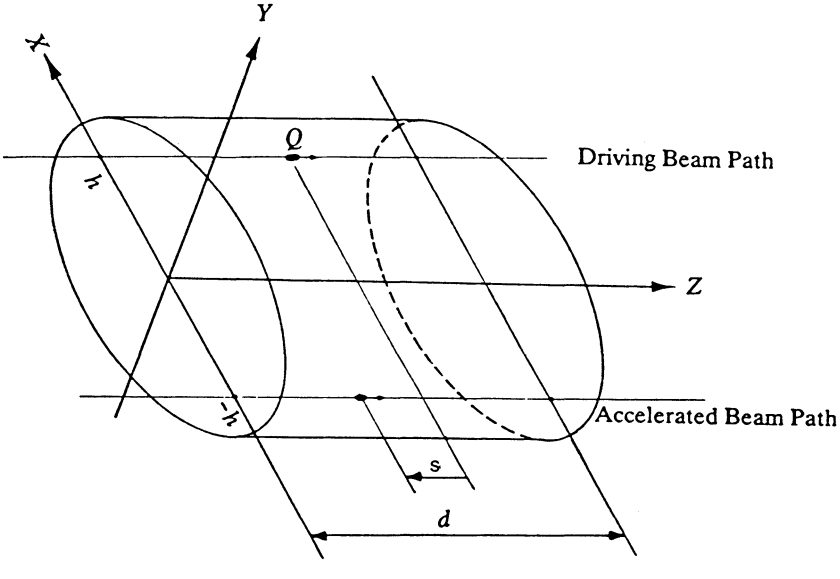

FIGURE 1 Elliptic pillbox cavity.

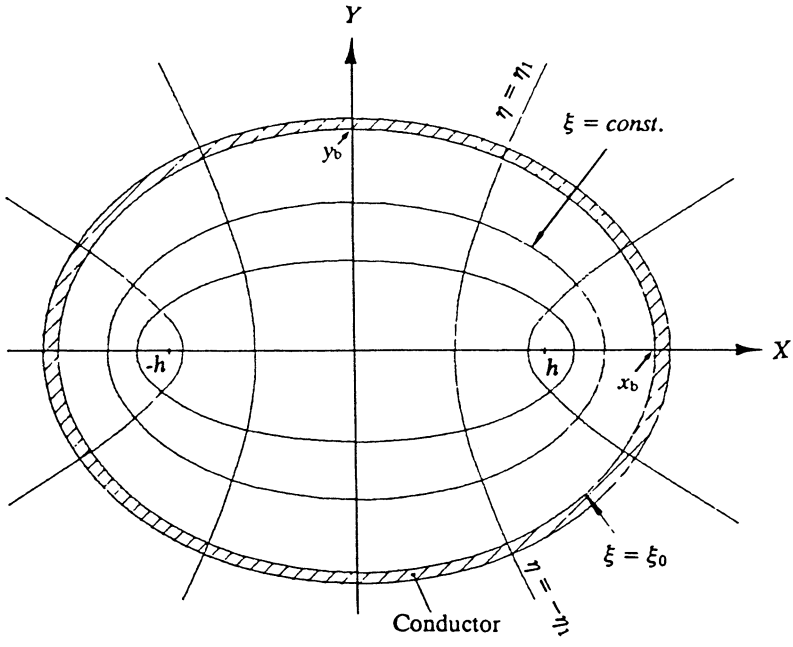

FIGURE 2 Confocal elliptical coordinates.

elliptic coordinate variables (ξ, η, z) are defined by[10]

$$\begin{aligned} X &= h \cosh \xi \cos \eta, \\ Y &= h \sinh \xi \sin \eta, \\ Z &= z, \end{aligned} \tag{1}$$

where h is the semi-interfocal distance.

The Helmholtz equation is then transformed to

$$\nabla^2\Psi + \kappa^2\Psi = \frac{1}{h^2(\sinh^2 \xi + \sin^2 \eta)}\left(\frac{\partial^2\Psi}{\partial\xi^2} + \frac{\partial^2\Psi}{\partial\eta^2}\right) + \frac{\partial^2\Psi}{\partial z^2} + \kappa^2\Psi = 0. \tag{2}$$

Following the method of separation of variables, we seek to find solutions of the form

$$\Psi(\xi, \eta, z) = f(\xi)g(\eta)w(z). \tag{3}$$

Substituting Eq. (3) into (2) and dividing by Ψ, Eq. (2) is split into three ordinary differential equations:

$$f''(\xi) - (a - 2q \cosh 2\xi)f(\xi) = 0, \tag{4}$$

$$g''(\eta) + (a - 2q \cos 2\eta)g(\eta) = 0, \tag{5}$$

$$w''(z) + \beta^2 w(z) = 0, \tag{6}$$

where $2q = \gamma^2 h^2/2$, $\gamma^2 = \kappa^2 - \beta^2$, and a is an arbitrary separation constant. The above Eqs. (4) and (5) are called the Mathieu equations. The solutions of these equations are the Mathieu functions[10].

2.2. Resonant Modes of a Cavity

For a closed elliptic pillbox cavity, we consider the solutions of

$$(\nabla_\perp^2 + \gamma^2)\psi(\xi, \eta) = 0 \tag{7}$$

in the region $0 \leq \xi \leq \xi_0$ and $0 \leq \eta \leq 2\pi$, where $\psi = E_z$ for a TM wave and H_z for a TE wave. Any combination of the product of the solution of Eqs. (4) and (5) is also the solution of Eq. (7). In addition to the boundary conditions, the following conditions must be satisfied:

(i) continuity of ψ on the interfocal line,

$$\psi(0, \eta) = \psi(0, -\eta), \tag{8}$$

(ii) continuity of gradient of ψ on the interfocal line,

$$\frac{\partial}{\partial \xi}(\psi(\xi, \eta))_{\xi \to 0} = -\frac{\partial}{\partial \xi}(\psi(\xi, -\eta))_{\xi \to 0}. \tag{9}$$

Among the possible combinations, the only permissible form of the solution which satisfies above two conditions is

$$\psi = \sum_{m=0}^{\infty} C_m Ce_m(\xi, q)ce_m(\eta, q) + \sum_{m=1}^{\infty} S_m Se_m(\xi, q)se_m(\eta, q), \tag{10}$$

with the factor $\exp(j(\omega t - \beta z))$ being omitted. Here, C_m and S_m are arbitrary constants. The functions $ce_m(\eta, q)$ and $se_m(\eta, q)$ are respectively the even and odd type Mathieu functions of the first kinds of integral order, and $Ce_m(\xi, q)$ and $Se_m(\xi, q)$ are the modified Mathieu functions of the first kinds of integral order. These functions are given by[10]

$$ce_{2n}(\eta, q) = \sum_{r=0}^{\infty} A_{2r}^{(2n)} \cos 2r\eta, \tag{11}$$

$$ce_{2n+1}(\eta, q) = \sum_{r=0}^{\infty} A_{2r+1}^{(2n+1)} \cos (2r + 1)\eta, \tag{12}$$

$$se_{2n+2}(\eta, q) = \sum_{r=0}^{\infty} B_{2r}^{(2n+2)} \sin (2r + 2)\eta, \tag{13}$$

$$se_{2n+1}(\eta, q) = \sum_{r=0}^{\infty} B_{2r+1}^{(2n+1)} \sin (2r + 1)\eta, \tag{14}$$

for $n = 0, 1, 2, \ldots$, and the coefficients A and B are function of q. Modified Mathieu functions $Ce_m(\xi, q)$ and $Se_m(\xi, q)$ have the same forms as in Eqs. (11)–(14) except η, sin, and cos are replaced by ξ, sinh, and cosh respectively.

We first notice that symmetry of $\psi(\xi, \eta)$ is determined by $ce_m(\eta, q)$ and $se_m(\eta, q)$. From Eqs. (11)–(14) we see that the first term in Eq. (10) is an even function and the second term is an odd function with respect to η. Therefore, the second term in Eq. (10) is always zero on the median plane ($y = 0$ plane) where wake potentials are to be evaluated, and does not contribute to the calculation of the longitudinal wake

potential. For this reason, we only consider the even-type modes of a TM wave, $\psi_m = Ce_m(\xi, q)ce_m(\eta, q)$, for the wake potential calculation.

The boundary conditions are:

$$\psi(\xi_0, \eta) = 0. \tag{15}$$

There remains the condition that no tangential component of electric field exists at the end-plate walls at $z = 0$ and d, which is satisfied if we choose

$$\beta = \frac{p\pi}{d}, \qquad p = 0, 1, 2, \ldots \tag{16}$$

where d is the gap distance of the pillbox cavity shown in Fig. 1. From Eq. (15) we have

$$Ce_m(\xi_0, q) = 0. \tag{17}$$

Let q_{mn} be the nth root of Eq. (17) for mode m. Then we can calculate the resonant frequencies from the root q_{mn}. Combining $2q = \gamma^2 h^2/2$ and $\gamma^2 = \kappa^2 - \beta^2$, the resonant frequencies are given by

$$\frac{\omega_{mnp}}{c} = \left\{\frac{4q_{mn}}{h^2} + \left(\frac{p\pi}{d}\right)^2\right\}^{1/2}. \tag{18}$$

The wavelength of the dominant mode is then given by

$$\lambda_{010} = \frac{\pi h}{\sqrt{q_{01}}} = \frac{\pi x_b e_c}{\sqrt{q_{01}}}, \tag{19}$$

where e_c and x_b are, respectively, the eccentricity and semi-major axis of the boundary ellipse. The ratio λ_{010}/x_b is plotted against e_c in Fig. 3. In this figure, we see that as $e_c \to 0$, i.e., as an ellipse tends to a circle, the ratio approaches 2.61, which is the ratio of wavelength to the radius, $\lambda/r_0 = 2\pi/\chi_{01}$, for the TM_{010} mode of a circular pillbox cavity of radius r_0, where χ_{01} is the first zero of Bessel function J_0.

The field components are given by

$$E_{z_{mnp}} = Ce_m(\xi, q_{mn})ce_m(\eta, q_{mn}) \cos\frac{p\pi}{d} z, \tag{20}$$

$$E_{\xi_{mnp}} = -\frac{p\pi}{D_{mn}d} Ce'_m(\xi, q_{mn})ce_m(\eta, q_{mn}) \sin\frac{p\pi}{d} z, \tag{21}$$

$$E_{\eta_{mnp}} = \frac{p\pi}{D_{mn}d} Ce_m(\xi, q_{mn})ce'_m(\eta, q_{mn}) \sin\frac{p\pi}{d} z, \tag{22}$$

$$H_{\xi_{mnp}} = \frac{j\omega_{mnp}\varepsilon_0}{D_{mn}d} Ce_m(\xi, q_{mn})ce'_m(\eta, q_{mn}) \cos\frac{p\pi}{d} z, \tag{23}$$

$$H_{\eta_{mnp}} = \frac{-j\omega_{mnp}\varepsilon_0}{D_{mn}d} Ce'_m(\xi, q_{mn})ce_m(\eta, q_{mn}) \cos\frac{p\pi}{d} z, \tag{24}$$

$$H_{z_{mnp}} = 0, \tag{25}$$

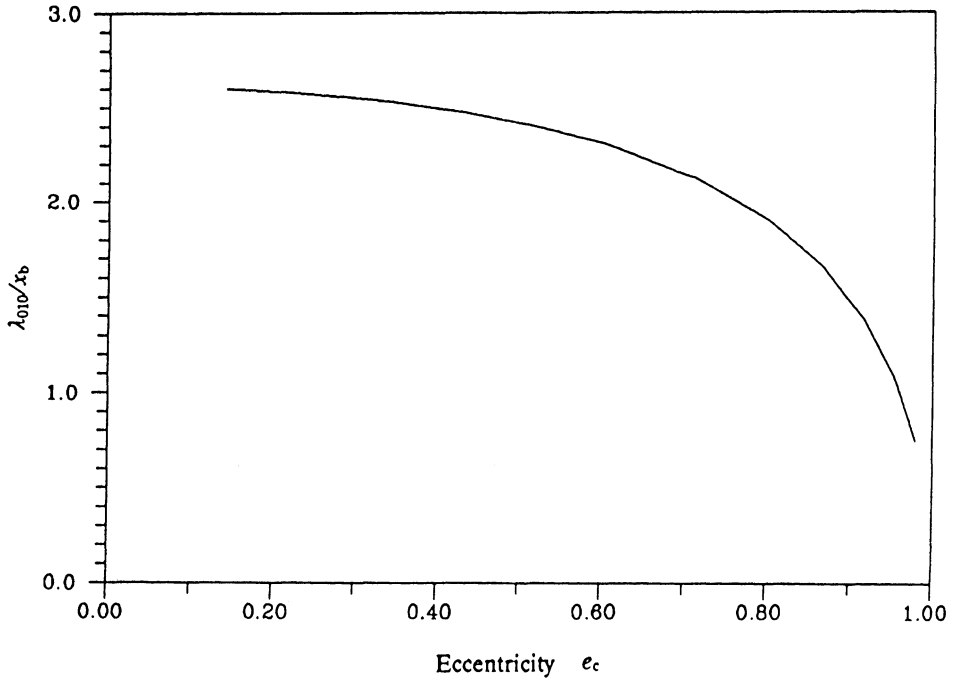

FIGURE 3 Plot of λ_{010}/x_b as a function of eccentricity.

where

$$D_{mn} = \frac{4q_{mn}}{h}\left\{\frac{\cosh 2\xi - \cos 2\eta}{2}\right\}^{1/2}. \tag{26}$$

The resonant mode patterns for some of the lower-order modes are shown in Fig. 4.

3. WAKE POTENTIAL CALCULATION

3.1. Longitudinal Wake Potential

Consider the test charge which is traveling through the focus axis of an elliptic pillbox cavity ($\xi = 0$, $\eta = \pi$) and trailing the driving charge Q, which is traveling through the other focus axis ($\xi = \eta = 0$), by a fixed distance s in the z-direction. The delta function longitudinal wake potential W_z is defined as the energy gained by unit test charge. Bane et al.[7] obtained the wake potential as an infinite sum

$$W_z(s) = 2\sum_{\lambda} k_\lambda \cos\left(\frac{\omega_\lambda s}{c}\right)$$

$$= \sum_{\lambda} \frac{V_\lambda^*(\mathbf{r}')V_\lambda(\mathbf{r})}{2u_\lambda} \cos\left(\frac{\omega_\lambda s}{c}\right), \qquad \text{for } s > 0 \tag{27}$$

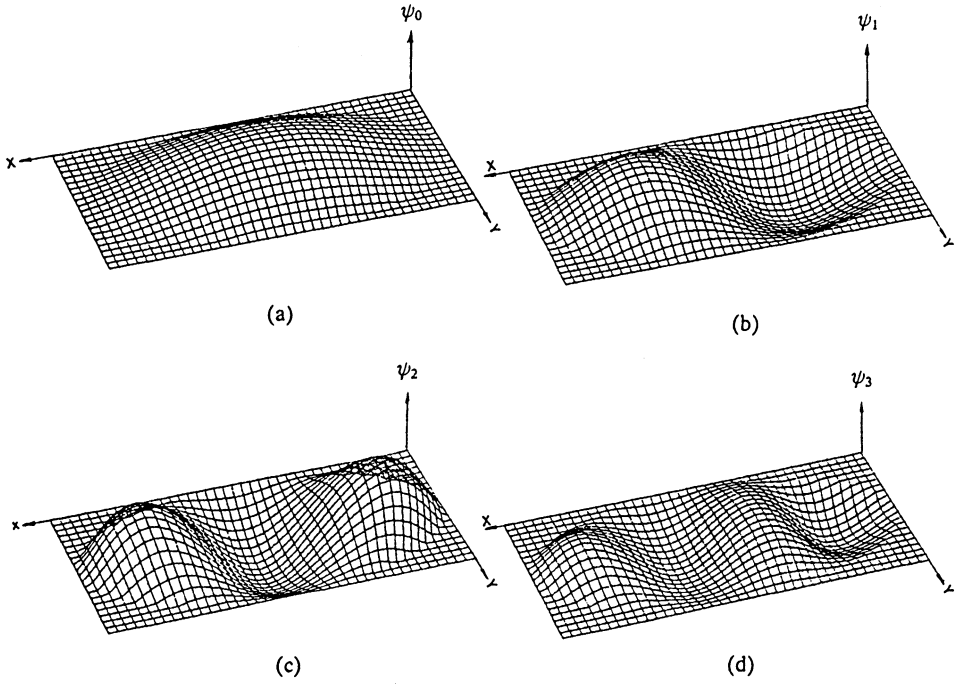

FIGURE 4 Configuration of resonant modes in an elliptic pillbox cavity. ((a) m = 0, (b) m = 1, (c) m = 2, (d) m = 3).

where k_λ is the loss parameter and V_λ is the voltage induced by a point charge Q. The stored energy u_λ is given by

$$\frac{\varepsilon_0}{2}\int \mathbf{a}_\lambda \cdot \mathbf{a}_{\lambda'}\, dV = u_\lambda \delta_{\lambda\lambda'}, \tag{28}$$

where $\mathbf{a}_\lambda$ is the vector eigenfunction. The vectors $\mathbf{r}'$ and $\mathbf{r}$ represent, respectively, the transverse position of the path of the driving charge and that of the test charge. Using the field components in Eqs. (20)–(22), the voltage V_λ becomes

$$\begin{aligned} V_\lambda(\mathbf{r}') &= \int_0^d dz \exp\left(\frac{j\omega z}{c}\right) a_{\lambda_z}(0, 0, z) \\ &= Ce_m(0, q_{mn}) ce_m(0, q_{mn}) \int_0^d dz \exp\left(\frac{j\omega z}{c}\right) \cos\frac{p\pi}{d} z, \end{aligned} \tag{29}$$

$$\begin{aligned} V_\lambda(\mathbf{r}) &= \int_0^d dz \exp\left(\frac{j\omega z}{c}\right) a_{\lambda_z}(\xi, \eta, z) \\ &= Ce_m(\xi, q_{mn}) ce_m(\eta, q_{mn}) \int_0^d dz \exp\left(\frac{j\omega z}{c}\right) \cos\frac{p\pi}{d} z, \end{aligned} \tag{30}$$

and further

$$V_\lambda^* V_\lambda = \frac{2C_{mn}\left(\frac{\omega}{c}\right)^2}{\left(\left(\frac{\omega}{c}\right)^2 - \left(\frac{p\pi}{d}\right)^2\right)^2}\left(1 - (-1)^p \cos\frac{\omega_{mnp} d}{c}\right), \tag{31}$$

where $C_{mn} = Ce_m(\xi, q_{mn})\, Ce_m(0, q_{mn})\, ce_m(\eta, q_{mn})\, ce_m(0, q_{mn})$.

The stored energy u_λ becomes

$$u_{mnp} = \frac{\varepsilon_0}{2}\int \mathbf{a}_\lambda \cdot \mathbf{a}_{\lambda'}\, dV$$

$$= \frac{\varepsilon_0}{2}\frac{\left(\frac{\omega_{mnp}}{c}\right)^2}{\gamma_{mn}^2}\int Ce_m^2(\xi, q_{mn}) ce_m^2(\eta, q_{mn}) \cos^2\left(\frac{p\pi}{d}\right) z\, dV. \tag{32}$$

After integration using $dV = \frac{h^2}{2}(\cosh 2\xi - \cos 2\eta)\, d\xi\, d\eta\, dz$, it is further reduced to

$$u_{mnp} = \frac{\varepsilon_0 \pi h^2 d}{8}\frac{\left(\frac{\omega_{mnp}}{c}\right)^2}{\gamma_{mn}^2}\int_0^{\xi_0} Ce_m^2(\xi, q_{mn}) \times (\cosh 2\xi - \Theta_m)\, d\xi, \tag{33}$$

where

$$\Theta_m = \frac{1}{\pi}\int_0^{2\pi} ce_m^2(\eta, q_{mn}) \cos 2\eta\, d\eta$$

$$= \begin{cases} A_0^{(m)} A_2^{(m)} + \sum_{r=0}^{\infty} A_{2r}^{(m)} A_{2r+2}^{(m)}, & \text{for } m = 0, 2, 4, \ldots \\ \frac{1}{2}(A_1^{(m)})^2 + \sum_{r=0}^{\infty} A_{2r+1}^{(m)} A_{2r+3}^{(m)}, & \text{for } m = 1, 3, 5, \ldots \end{cases} \tag{34}$$

and $A_r^{(m)}$ are the coefficients for the series representation of the Mathieu function $ce_m(\eta, q)$ given in Eqs. (11) and (12).

Substituting Eq. (31) and (33) into (27), the delta function longitudinal wake potential on the accelerated beam path ($\xi = 0, \eta = \pi$) becomes

$$W_z(s) = \frac{2}{\varepsilon_0 \pi d}\sum_{m=0}^{\infty}\sum_{n=1}^{\infty}\sum_{p=0}^{\infty}\frac{\varepsilon_p C_{mn}\left(1 - (-1)^p \cos\frac{\omega_{mnp} d}{c}\right)}{q_{mn} N_{mn}} \cos\left(\frac{\omega_{mnp} s}{c}\right), \tag{35}$$

where $\varepsilon_p = \frac{1}{2}$ for $p = 0$ and 1 for $p \neq 0$. N_{mn} and C_{mn} in Eq. (35) are given by

$$N_{mn} = \int_0^{\xi_0} Ce_m^2(\xi, q_{mn}) \times (\cosh 2\xi - \Theta_m)\, d\xi, \tag{36}$$

$$C_{mn} = (Ce_m(0, q_{mn}))^2 ce_m(0, q_{mn}) ce_m(\pi, q_{mn})$$
$$= \begin{cases} \left(\sum_{r=0}^{\infty} A_{2r}^{(m)}\right)^4 & \text{for } m = 0, 2, 4, \ldots \\ -\left(\sum_{r=0}^{\infty} A_{2r+1}^{(m)}\right)^4 & \text{for } m = 1, 3, 5, \ldots \end{cases} \tag{37}$$

For a circular pillbox cavity, W_z is expressed analytically[7,8] in the form of

$$W_z(s) = \frac{4}{\varepsilon_0 \pi d} \sum_{n=1}^{\infty} \sum_{p=0}^{\infty} \varepsilon_p \frac{\left(1 - (-1)^p \cos \frac{\omega_{onp} d}{c}\right)}{\chi_{on} J_1^2(\chi_{on})} \cos\left(\frac{\omega_{onp} s}{c}\right), \tag{38}$$

where χ_{on} is the nth zero of the Bessel function J_0.

When the boundary ellipse tends to a circle of radius r_0, the confocal hyperbolae in Fig. 2 become radii of the circle r, and the confocal ellipses become concentric circles of that radius. In this case, Eq. (35) is reduced exactly to Eq. (38). We can easily show this by using the limiting properties of Mathieu functions. The Mathieu functions $ce_m(\eta, q)$ and $Ce_m(\xi, q)$ degenerate into the following forms[10] as $h \to 0$ and $\xi \to \infty$, while keeping the product $h \cosh \xi \to r$:

$$q \to 0 \quad \text{as} \quad h \to 0, \tag{39}$$

$$ce_m(\eta, q) \to \begin{cases} \sqrt{\frac{1}{2}}, & \text{for } m = 0 \\ \cos m\phi, & \text{for } m \neq 0 \end{cases} \tag{41}$$

$$Ce_m(\xi, q) \to p_m J_m(\gamma r), \tag{41}$$

$$A_r^{(m)} \to 0 \text{ (except } A_m^{(m)} \to 1 \text{ for } m \neq 0, \text{ and } A_0^{(0)} \to \sqrt{\tfrac{1}{2}}), \tag{42}$$

where p_m is a constant multiplier, and $J_m(x)$ is the Bessel function of the first kind. Then, Eq. (37) becomes

$$C_{mn} = (Ce_m(0, q_{mn}))^2 ce_m(0, q_{mn}) ce_m(\pi, q_{mn})$$
$$\to (p_m J_m(0) \cos m\phi)^2 = 0, \quad \text{for } m \neq 0$$
$$\to (p_0 J_0(0))^2/2 = p_0^2/2, \quad \text{for } m = 0. \tag{43}$$

It is apparent from Eq. (43) that contributions from $m \neq 0$ modes become zero as expected as an ellipse tends to a circle. The denominator in Eq. (35) for $m = 0$ becomes

$$q_{on} \int_0^{\xi_0} Ce_0^2(\xi, q_{on}) \cosh 2\xi \, d\xi \to \frac{(p_0 \gamma)^2}{2} \int_0^{r_0} J_0^2(\gamma r) r \, dr$$
$$\to \frac{p_0^2}{4} \chi_{on}^2 J_1^2(\chi_{on}), \tag{44}$$

where $\gamma = \chi_{on}/r_0$. Substituting Eqs. (43) and (44) into (35), we can get exactly the same expression for the wake potential in the circular pillbox cavity as in Eq. (38).

No closed expression is known for the infinite sum in Eqs. (35) and (38), and they must be evaluated numerically.

If the driving bunch has a Gaussian charge distribution

$$\lambda(z) = \frac{1}{\sqrt{2\pi}\sigma} \exp\left(\frac{-z^2}{2\sigma^2}\right), \tag{45}$$

then the bunch wake potential U_z becomes

$$\begin{aligned} U_z(s) &= \int_{-\infty}^{s} \lambda(z) W_z(s-z)\, dz \\ &= \frac{\sqrt{2/\pi}}{\varepsilon_0 \pi\, d\sigma} \sum_{m=0}^{\infty} \sum_{n=1}^{\infty} \sum_{p=0}^{\infty} \frac{\varepsilon_p C_{mn}\left(1-(-1)^p \cos\dfrac{\omega_{mnp} d}{c}\right)}{q_{mn} N_{mn}} \\ &\quad \times \int_{-\infty}^{s} \exp\left(\frac{-z^2}{2\sigma^2}\right) \cos\frac{\omega_{mnp}(s-z)}{c}\, dz. \end{aligned} \tag{46}$$

When $s \gg \sigma$, the bunch wake potential becomes

$$\begin{aligned} U_z(s) &\approx \frac{2}{\varepsilon_0 \pi d} \sum_{m=0}^{\infty} \sum_{n=1}^{\infty} \sum_{p=0}^{\infty} \exp\left(-\left(\frac{\omega_{mnp}}{c}\right)^2 \sigma^2/2\right) \\ &\quad \times \frac{\varepsilon_p C_{mn}\left(1-(-1)^p \cos\dfrac{\omega_{mnp} d}{c}\right)}{q_{mn} N_{mn}} \cos\frac{\omega_{mnp} s}{c}. \end{aligned} \tag{47}$$

From this equation, we can see that contributions from the modes whose resonant wavelengths are much shorter than the bunch length 2σ become negligible. For the dominant mode, Eq. (47) can be conveniently written as

$$U_{z_{010}} \approx \frac{(1-e_c^2)^{1/2} \lambda^2 C_{01}}{\varepsilon_0 \pi^2 d e_c^2 S N_{01}} e^{-1/2(2\pi\sigma/\lambda)^2}\left(1-\cos\frac{2\pi d}{\lambda}\right)\cos\frac{2\pi s}{\lambda}, \tag{48}$$

where $S = \pi x_b y_b$ is the cross sectional area of the cavity, λ is the wavelength of dominant mode, and e_c is the eccentricity of the boundary ellipse. From Eq. (48), we see that the wake potential scales as ω_λ^{-2} and S^{-1}.

3.2. *Transverse Wake Potential*

From the Panofsky–Wenzel theorem, the transverse wake potential is related to the longitudinal wake potential by

$$\frac{\partial \mathbf{W}_\perp(s)}{\partial s} = \nabla_\perp W_z(s). \tag{49}$$

From this relation we can write the transverse delta function wake potential as[7]

$$\mathbf{W}_\perp(s) = \sum_\lambda c \frac{V_\lambda^*(\mathbf{r}') \nabla_\perp V_\lambda(\mathbf{r})}{2 u_\lambda \omega_\lambda} \sin\left(\frac{\omega_\lambda s}{c}\right). \tag{50}$$

On the accelerating beam path ($\xi = 0, \eta = \pi$), we have

$$V_\lambda^*(\mathbf{r}')\nabla_\perp V_\lambda(\mathbf{r}) = Ce_m(0, q_\lambda)ce_m(0, q_\lambda)ce_m(\pi, q_\lambda)\nabla_\perp Ce_m(0, q_\lambda) \times \left(\int_0^d dz \exp\left(\frac{j\omega z}{c}\right) \cos\frac{p\pi}{d} z\right)^2. \tag{51}$$

Since the driving charge and test charge are assumed to pass through each focus axis, only $\hat{\xi}$-component of the transverse wake potential exists at the foci of the elliptic cavity. Thus,

$$\nabla_\perp Ce_m(0, q_\lambda) = \hat{\xi} \lim_{\xi \to 0} \frac{1}{h \sinh \xi} \frac{\partial}{\partial \xi} Ce_m(\xi, q_\lambda) = \hat{\xi} \begin{cases} \frac{1}{h} \sum_{r=0}^{\infty} (2r)^2 A_{2r}^{(m)}, & \text{for } m = 0, 2, 4, \ldots \\ \frac{1}{h} \sum_{r=0}^{\infty} (2r+1)^2 A_{2r+1}^{(m)}, & \text{for } m = 1, 2, 5, \ldots \end{cases} \tag{52}$$

Therefore, the transverse delta function wake potential is given by

$$W_\perp(s) = \frac{2c}{\varepsilon_0 \pi d} \sum_\lambda \frac{\varepsilon_p \bar{C}_\lambda \left(1 - (-1)^p \cos\frac{\omega_\lambda d}{c}\right)}{\omega_\lambda q_\lambda N_\lambda} \sin\left(\frac{\omega_\lambda}{c} s\right), \tag{53}$$

where

$$\bar{C}_\lambda = Ce_m(0, q_{mn})ce_m(0, q_{mn})ce_m(\pi, q_{mn})\nabla_\perp Ce_m(0, q_{mn}) = \begin{cases} \frac{1}{h}\left(\sum_{r=0}^{\infty} A_{2r}^{(m)}\right)^3 \left(\sum_{r=0}^{\infty} (2r)^2 A_{2r}^{(m)}\right), & \text{for } m = 0, 2, 4, \ldots \\ \frac{-1}{h}\left(\sum_{r=0}^{\infty} A_{2r+1}^{(m)}\right)^3 \left(\sum_{r=0}^{\infty} (2r+1)^2 A_{2r+1}^{(m)}\right), & \text{for } m = 1, 3, 5, \ldots \end{cases} \tag{54}$$

For the driving bunch of a Gaussian charge distribution, the transverse bunch wake potential becomes

$$U_\perp(s) = \int_{-\infty}^{s} \lambda(z) W_\perp(s - z)\, dz = \frac{c\sqrt{2/\pi}}{\varepsilon_0 \pi d\sigma} \sum_{m=0}^{\infty} \sum_{n=1}^{\infty} \sum_{p=0}^{\infty} \frac{\varepsilon_p \bar{C}_{mn} \left(1 - (-1)^p \cos\frac{\omega_{mnp} d}{c}\right)}{\omega_{mnp} q_{mn} N_{mn}} \times \int_{-\infty}^{s} \exp\left(\frac{-z^2}{2\sigma^2}\right) \sin\frac{\omega_{mnp}}{c} (s - z)\, dz. \tag{55}$$

4. NUMERICAL EXAMPLES AND DISCUSSIONS

The longitudinal and transverse wake potentials in an elliptic pillbox cavity are calculated by using Eqs. (46) and (55). We choose the same cavity dimensions and bunch length as in Ref. 9 to compare the results. The cavity dimensions and beam parameter are:

$$\text{major axis } 2x_b = 10 \text{ cm},$$
$$\text{minor axis } 2y_b = 6 \text{ cm},$$
$$\text{gap distance } d = 2 \text{ cm},$$
$$\sigma = 5 \text{ mm}.$$

The wavelength, λ_{mnp}, and the loss parameters of a Gaussian bunch, $k_\lambda(\sigma)$, for some of lower-order resonant modes are tabulated in Table I, while in Table II the

TABLE I

Wavelength λ_{mnp} and Loss Parameter $k_{mnp}(\sigma)$ of an Elliptical Pillbox Cavity ($x_b = 5$ cm, $y_b = 3$ cm, $d = 2$ cm, $\sigma = 5$ mm)

m	q_{m1}	λ_{m10} (cm)	λ_{m11} (cm)	λ_{m12} (cm)	$k_{m10}(\sigma)$ (V/pC)	$k_{m11}(\sigma)$ (V/pC)	$k_{m12}(\sigma)$ (V/pC)
0	1.7353	9.5394	3.6883	1.9574	3.2345×10^{-2}	1.6366×10^{-3}	6.8638×10^{-5}
1	3.3522	6.8634	3.4559	1.9201	1.2629×10^{-1}	1.2993×10^{-2}	5.7848×10^{-4}
2	5.6530	5.2853	3.1895	1.8705	2.2821×10^{-1}	4.3203×10^{-2}	2.0914×10^{-3}
3	8.6577	4.2708	2.9194	1.8112	2.5776×10^{-1}	8.4739×10^{-2}	4.5668×10^{-3}
4	12.3689	3.5731	2.6648	1.7452	2.0007×10^{-1}	1.1262×10^{-1}	6.9154×10^{-3}
5	16.7792	3.0678	2.4343	1.6754	1.1060×10^{-1}	1.0854×10^{-1}	7.7733×10^{-3}

m	q_{m2}	λ_{m20} (cm)	λ_{m21} (cm)	λ_{m22} (cm)	$k_{m20}(\sigma)$ (V/pC)	$k_{m21}(\sigma)$ (V/pC)	$k_{m22}(\sigma)$ (V/pC)
0	11.3563	3.7289	2.7276	1.7625	2.8997×10^{-6}	1.4188×10^{-6}	8.4089×10^{-8}
1	14.6278	3.2856	2.5389	1.7084	1.9755×10^{-5}	1.4828×10^{-5}	9.8517×10^{-7}
2	18.4878	2.9225	2.3598	1.6505	6.1309×10^{-5}	7.4392×10^{-5}	5.6547×10^{-6}
3	22.9665	2.6221	2.1930	1.5902	1.0984×10^{-4}	2.3849×10^{-4}	2.1224×10^{-5}
4	28.0957	2.3708	2.0395	1.5287	1.1261×10^{-4}	5.4398×10^{-4}	5.8271×10^{-5}
5	33.9196	2.1577	1.8990	1.4668	4.5322×10^{-4}	9.1853×10^{-4}	1.2279×10^{-5}

TABLE II

Wavelength λ_{onp} and Loss Parameter $k_{onp}(\sigma)$ of a Circular Pillbox Cavity ($r_0 = 3.873$ cm, $d = 2$ cm, $\sigma = 5$ mm)

n	χ_{on}	λ_{ono} (cm)	λ_{on1} (cm)	λ_{on2} (cm)	$k_{on0}(\sigma)$ (V/pC)	$k_{on1}(\sigma)$ (V/pC)	$k_{on2}(\sigma)$ (V/pC)
1	2.405	10.118	3.720	1.962	7.235×10^{-1}	3.212×10^{-2}	1.338×10^{-3}
2	5.520	4.408	2.962	1.821	6.031×10^{-1}	1.818×10^{-1}	9.614×10^{-3}
3	8.654	2.812	2.300	1.630	1.162×10^{-1}	1.700×10^{-1}	1.361×10^{-2}
4	11.792	2.064	1.834	1.436	4.419×10^{-4}	4.693×10^{-2}	7.128×10^{-3}
5	14.931	1.630	1.509	1.263	3.944×10^{-3}	2.710×10^{-3}	1.458×10^{-3}

same information is given for the circular pillbox cavity that has the same cross sectional area ($r_0 = \sqrt{x_b y_b}$).

Figures 5 and 6 are, respectively, the curves of the longitudinal wake potential on the accelerated beam path and that on the driving beam path, in which different number of modes are included (solid lines for 24 modes and broken lines for 12 modes). From these figures, we see that the mode summation converges rapidly, indicating clearly that the wake potential is dominated by a few lower modes. It was pointed out that the wake potential inside the bunch is difficult to calculate because of the slow convergence of mode summation[8]. However, it is not clear in these figures whether the series converges rather slowly for positions inside the driving bunch.

On the accelerated beam path, we obtained about 125 MeV/m/μC acceleration gradient, while about 110 MeV/m/μC was obtained by Y. Chin[9] (see Fig. 7). The elliptical cavity in this example calculation does not represent the maximum acceleration gradient that can be achieved. As discussed earlier, the longitudinal wake potential is proportional to the number of particles in the driving bunch and inversely proportional to the cross sectional area of the cavity. Also, it is dependent on the distribution of charges within a bunch and the eccentricity of a cavity. By choosing appropriate parameters, one can achieve an even-higher acceleration gradient.

The transverse wake potentials on the accelerated beam path and driving beam path are shown in Figs. 8 and 9 by the broken lines. The corresponding longitudinal

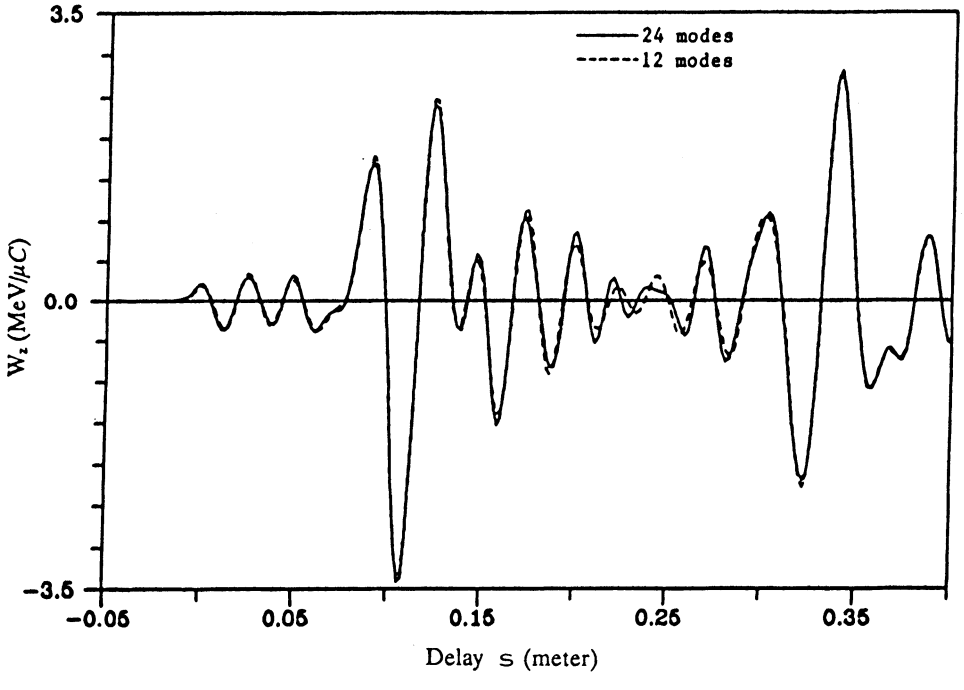

FIGURE 5 Plot of the longitudinal wake potential on the accelerated beam path (solid line: 24 modes sum; broken line: 12 modes sum).

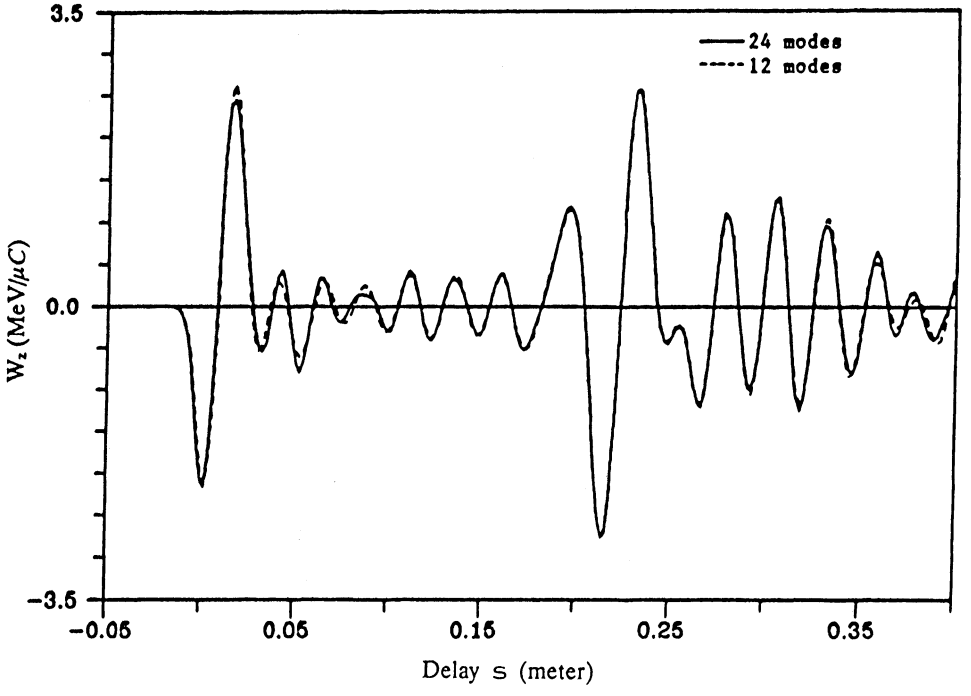

FIGURE 6 Plot of the longitudinal wake potential on the driving beam path (solid line: 24 modes sum; broken line: 12 modes sum).

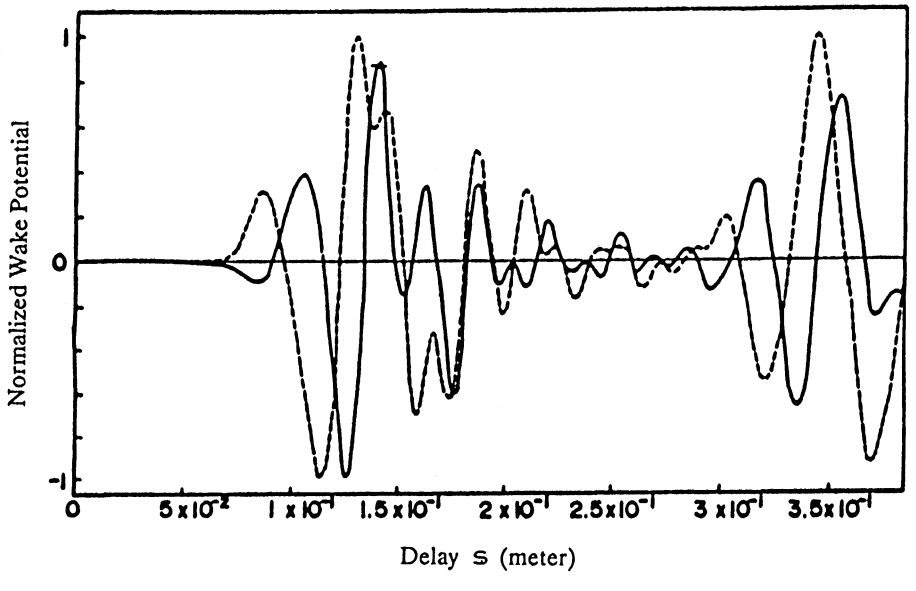

FIGURE 7 Plot of normalized wake potentials on the accelerated beam path (results of Ref. 9, solid line: longitudinal wake potential/(2.54 MeV/μC); broken line: transverse wake potential/(1.11 MeV/μC)).

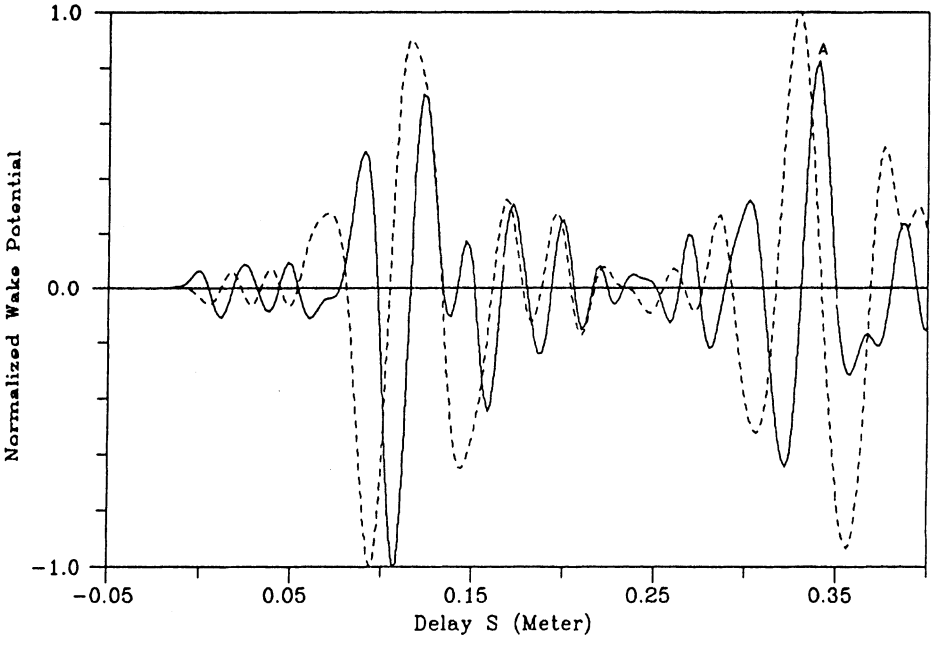

FIGURE 8 Plot of normalized wake potentials on the accelerated beam path (solid line: longitudinal wake potential (3.40 MeV/μC); broken line: transverse wake potential (1.29 MeV/μC)).

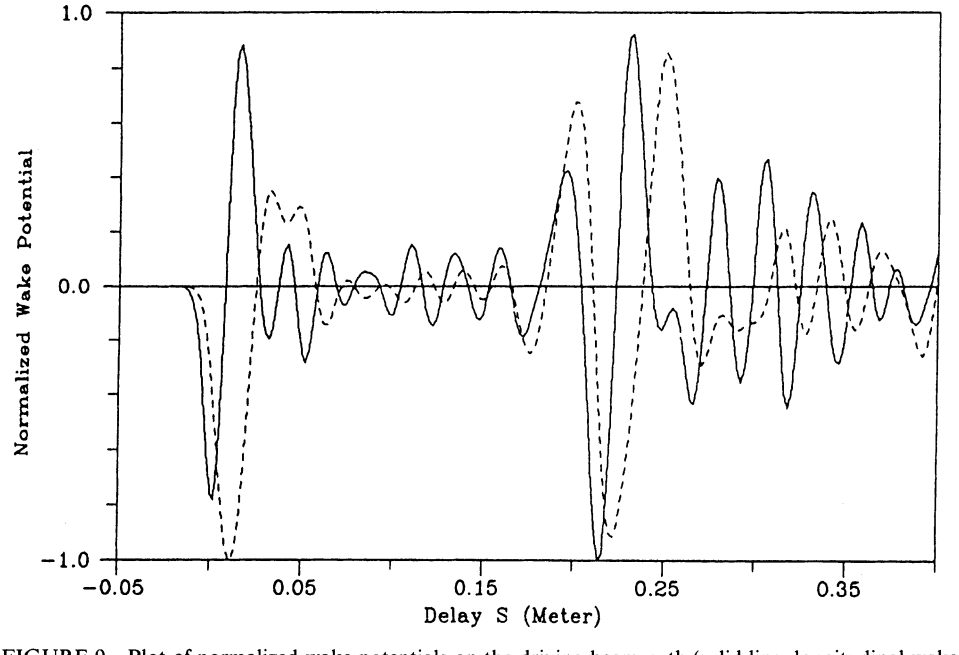

FIGURE 9 Plot of normalized wake potentials on the driving beam path (solid line: longitudinal wake potential (2.77 MeV/μC); broken line: transverse wake potential (1.68 MeV/μC)).

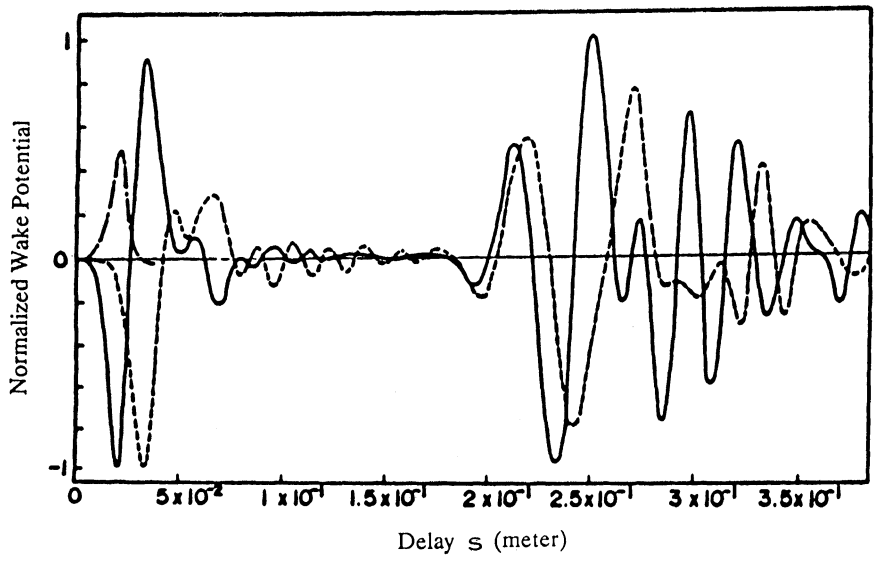

FIGURE 10 Plot of normalized wake potentials on the driving beam path (results of Ref. 9, solid line: longitudinal wake potential/(1.92 MeV/μC); broken line: transverse wake potential/(1.48 MeV/μC)).

wake potentials are plotted together in order to see if we can find the positions, such as the point A in Fig. 8, at which the accelerating potential is large while the transverse potential is small. The charge to be accelerated should be positioned at such a point in order to avoid large transverse deflection during acceleration. Figures 7 and 10 are, respectively, the curves for the longitudinal and transverse wake potentials on the accelerated beam path and driving beam path calculated by the numerical code WELL[9]. In these calculations, the effect of beam apertures of 0.5 cm radius was considered. Comparing these analytical results (Figures 8 and 9) with numerical method (Figures 7 and 10), we found very good agreement in both magnitudes and frequencies. However, magnitude of the longitudinal and transverse wake potentials are higher for this analytical method which does not include the beam aperture effects.

ACKNOWLEDGMENTS

This work is supported in part by the U.S. Air Force Office of Science Research under grant no. AFOSR-87-0280.

REFERENCES

1. G. A. Voss and T. Weiland, DESY reports M82-10 (1982) and M82-074 (1982).
2. S. H. Kim, J. Plasma Phys. **36**, 195 (1986); Corrigendum **41**, 577 (1989); S. H. Kim, Phys. Lett. **135A**, 39 (1989).
3. H. Figueroa, W. Gai, R. Konecny, J. Norem, A. Ruggiero, P. Schoessow, and J. Simpson, Phys. Rev. Lett. **60**, 21 (1988).

4. J. B. Rosenzweig, D. B. Cline, B. Cole, H. Figueroa, W. Gai, R. Konecny, J. Norem, P. Schoessow and J. Simpson, Phys. Lett. **61**, 98 (1988).
5. W. Gai, P. Schoessow, B. Cole, R. Konecny, J. Norem, J. Rosenzweig, and J. Simpson, Phys. Lett. **61**, 2756 (1988).
6. K. W. Chen and S. H. Kim, *Proc. of 6th International Conference on High Power Particle Beams*, Kobe, Japan (June 1986).
7. K. L. F. Bane, P. B. Wilson, and T. Weiland, in *Physics of High Energy Particle Accelerators*, AIP Conf. Proc. No. 127, AIP, New York (1983).
8. T. Weiland and B. Zotter, Part. Accel. **11**, 143–151 (1981).
9. Y. Chin, KEK report 83–19 (1983).
10. N. W. McLachlan, *Theory and Application of Mathieu Functions*, Dover Publications, Inc., NY (1964).